Durá, JL.; Solanes, C.; De Andrés, J.; Saiz Rodríguez, FJ. (2019). Computational Study of the Effect of Electrode Polarity on Neural Activation Related to Paresthesia Coverage in Spinal Cord Stimulation Therapy. Neuromodulation: Technology at the Neural Interface. 22(3):269-279. https://doi.org/10.1111/ner.12909

ABSTRACT

Objective: Using computer simulation, we investigated the effect of electrode polarity on neural activation in spinal cord stimulation (SCS) and propose a new strategy to maximize the activating area in the dorsal column (DC) and, thus, paresthesia coverage in clinical practice.

Materials and Methods: A new 3D spinal cord model at the T10 vertebral level was developed to simulate neural activation induced by the electric field distribution produced by different typical four-contact electrode polarities in single- and dual-lead stimulation. Our approach consisted of the combination of a finite element model of the spinal cord developed in COMSOL Multiphysics and a nerve fiber model implemented in MATLAB. Five evaluation parameters were evaluated, namely, the recruitment ratio, the perception and discomfort thresholds, and the activating area and depth. The results were compared quantitatively.

Results: The dual-guarded cathode presents the maximum activating area and depth in single- and dual-lead stimulation. However, the lowest value of the ratio between the perception threshold in DC and the perception threshold in the dorsal root (DR) is achieved when the guarded cathode is programmed. Although the two versions of bipolar polarity (namely bipolar 1 and bipolar 2) produce higher activating area and depth than the guarded cathode, they are suitable for producing DR stimulation. Similarly, dual-lead stimulation is likely to activate DR fibers because the electrodes are closer to these fibers.

Conclusions: The results suggest that the activating area in the DC is maximized by using the dual-guarded cathode both in single- and dual-lead stimulation modes. However, DC nerve fibers are preferentially stimulated when the guarded cathode is used. According to these results, the new electrode programming strategy that we propose for clinical practice first uses the dual-guarded cathode, but, if the DR nerve fibers are activated, it then uses guarded cathode polarity.

KEY WORDS: *dorsal column stimulation, dorsal root stimulation, electrode polarity, computational model, spinal cord stimulation.*

INTRODUCTION

Spinal cord stimulation (SCS) is a well-established clinical technique for the treatment of various chronic pain–associated syndromes (1–6). This technique involves the delivery of electric current to the spinal cord via electrodes placed in the dorsal epidural space. Connected to a pulse generator, the electrodes can be programmed as either anodes (positive potential) or cathodes (negative potential) to generate an electric field that stimulates neural elements (7).

The neurophysiological mechanisms involved in SCS were first described by Melzack and Wall through the gate control theory of pain (8). These authors postulated that by selectively activating Aβ fibers by electrical stimulation, the "gate" could be electively closed, thus reducing painful inputs toward the brain and eliciting a tingling sensation (paresthesia) in pain dermatomes (9–11). Other subsequently proposed mechanisms of action maintain the same necessary condition of Aβ fiber stimulation to overlap the sensation of paresthesia on the perceived areas of pain (12).

Large Aβ nerve fibers are located in the dorsal column (DC) and dorsal root (DR). Although pain relief may be elicited by Aβ nerve fiber stimulation in both structures, DR stimulation can only induce paresthesia in a few dermatomes, whereas DC stimulation can induce it in many dermatomes (13). And, the induction of paresthesia in many dermatomes is a necessary condition for the success of SCS in complex pain syndromes.

For decades, computational models of SCS have been fundamental to the understanding of clinical observations and the design of therapies with optimal results (14). Computational models use the finite element method (FEM) to find only an approximate solution to the problem. The advantage

of the FEM is that the solution region is considered to be built up of many small, interconnected sub-regions (finite elements), thus enabling the problem to be replaced by a simpler one when attempting to find a solution (15). Therefore, the best known FEM model of SCS was developed by Holsheimer (16), whose main studies were related to the neural structures involved in inducing paresthesia and the effect of electrode configuration on their activation (11,17–20). However, next-generation computational models were more sophisticated, and studies were focused on the effect of the stimulation parameters on neural stimulation (14). The four basic parameters which need to be programmed in SCS are amplitude, pulse width, frequency, and polarity, whose combination satisfies an individual's pain coverage needs (21). As for polarity, Holsheimer and Wesselink suggested that guarded cathode polarity produced the deepest and widest paresthesia coverage, although no quantitative parameters were evaluated (22). Furthermore, since percutaneous electrodes have from four to eight poles, a huge number of combinations can be used. For instance, 6,558 combinations can be used when using two four-contact stimulation electrodes. Thus, in clinical practice, polarity is determined by eliciting the patient's oral responses to the trial and error–based application of stimulation, which may be time-consuming. For these reasons, the goals of the present study were to quantitatively investigate the effect of electrode polarity on neural activation using a new 3D spinal cord model developed by our group and to propose a new strategy to maximize paresthesia coverage in clinical practice.

MATERIALS AND METHODS

Volume conductor model of the spinal cord

We created a 3D volume conductor model of the spinal cord at the T10 level using real geometric parameters from a magnetic resonance imaging (MRI) study of the human spinal cords of 15 volunteers aged 20-40 years (23). The measurements considered were the following: the anteroposterior diameter of the white matter (ØAP), the transverse diameter of the white matter

(ØT), and the distance between the dura mater and spinal cord in the anterior (A), posterior (P), right (R), and left (L) directions (see Figure 1(a) and (b)). All measurements were taken in the prone position. A FEM model was created in COMSOL Multiphysics (version 5.3) and included the following tissues: cerebrospinal fluid (CSF), grey and white matter, dura mater, fat, DRs, and bone (see Figure 1(a) and (b)). In our model, dura mater has a thickness of 0.3 mm (24), fat tissue 4 mm (25), and bone 10 mm. The electrical tissue conductivities considered were obtained from (6,9,26–29) (see Table 1). The volume conductor model measured 45 (*x*) mm × 42 (*y*) mm × 44 (*z*) mm (see Figure 1(d)).

We included a 3D representation of the DR, based on the DR model of Sankarasubramanian (30). To be more realistic, we included 80 DRs spaced 1 mm apart throughout the longitudinal axis of the volume conductor model (see Figure 1(c)). The purpose of this overpopulation of DR fibers was to ensure that the lowest DR stimulation threshold could be determined and to minimize the effect of the relative position of the cathode with respect to the DR in the longitudinal axis.

We used a tetrahedral adaptive mesh to avoid incorrect solutions in the narrow and edge zones of the model. The element size ranged from 0.067 to 1.57 mm. The model used approximately 2,000,000 nodes. However, the number of mesh elements varied according to the number of electrodes used in the model. Thus, the model had 1,536,452 elements with one lead and 1,660,187 elements with two leads. All mesh properties are shown in Table 2.

With the aim of preventing possible edge effects, we imposed the Dirichlet boundary condition (electric insulation) on the most external surfaces of the model. We also imposed an electric potential boundary on the surfaces of the active contacts of the electrode. Table 2 shows the boundary conditions applied to the model.

The FEM was used for the calculation of the electrical potential distribution as an approximate solution of the Laplace equation ($\nabla^2 V = 0$). The current density ($\boldsymbol{J}$(x,y,z)) was obtained from the generalized version of Ohm's Law (Equations (1) and (2)):

$$\boldsymbol{J} = \sigma * \boldsymbol{E} \qquad (1)$$

$$\boldsymbol{E} = -\nabla V_e, \qquad (2)$$

where V_e is the electrical potential of a specific point of the volume conductor model, $\boldsymbol{E}$ is the electric field, $\boldsymbol{J}$ is the current density, and σ is the electrical conductivity tensor. The electric field, the electric potential, and the electric current were calculated using the conjugate gradient iterative method solver (31). All simulations were run as static models.

Percutaneous lead model

We modeled multipole percutaneous leads, including the electrode contacts, the insulation, and the electrode-tissue interface. Usually, percutaneous leads have eight contacts, but we only included four contacts in the model because, in our clinical practice, no more than four consecutive contacts are programmed. Despite the availability of different percutaneous lead sizes, we only used one lead size because we wished to see the effect of polarity and not the effect of lead geometry on neural activation. The geometry we used can be seen in (32). The electrodes were then modeled as cylinders measuring 24 mm in length and 1.3 mm in diameter. The contacts (conducting domains) had a length of 3 mm and were spaced 4 mm apart with the application of an insulating polymer (non-conductive domains). The insulator at the extremes of the electrodes had a length of 1.5 mm (see Figure 3(c)). Moreover, we included the electrode-tissue interface as a hollow cylinder with a 0.1-mm thickness, which covered the active contacts. To date, this structure has only been considered in a deep brain stimulation model developed by Butson et al. (33,34).

Finally, the percutaneous lead model was positioned in the midline of the transversal plane of the model in single-lead stimulation or 1.25 mm from the midline to the axis of the electrode in dual-lead stimulation. In both cases, the electrodes were 0.1 mm from the dura mater.

Myelinated nerve fiber model

In order to determine nerve fiber activation (in the DC or DR), we used the McIntyre, Richardson, and Grill (MRG) myelinated nerve fiber model (35). The model was implemented using MATLAB R2017a. We used model B because its conduction velocity (61 ms^{-1}) was within the experimental range for a 10-µm fiber (47-63 ms^{-1}) (34). The model incorporates a finite impedance single-cable myelin sheath. This is important, because representation of myelin is a significant factor in axon excitability and conduction (34). The electrical representation for both the myelin and nodes of Ranvier are shown in Figure 2(a). The MRG model allows for the calculation of the membrane potential in each node of Ranvier (V_n), taking into account V_e values obtained from Equation (2), by solving the following equation:

$$\frac{dV_n}{dt} = \frac{1}{C_{m,n}}\left[-I_{ion,n} + G_{axial}(V_{n-1} - 2V_n + V_{n+1} + V_{e,n-1} - 2V_{e,n} + V_{e,n+1})\right], \qquad (3)$$

where n is the corresponding node of Ranvier, C_m is the membrane capacity (μF), I_{ion} is the total sum of the ionic currents (mA), and G_{axial} is the conductance between the centers of two adjacent compartments (mS). For more details about MRG model equations, see Richardson et al. (35), and for details of the geometric parameters, see McIntyre et al. (36). All the parameters used in the model are also shown in Table S1-S4 of the Supporting Information section. When Equation (3) is solved for each node of Ranvier, we obtain the temporal evolution of the membrane potential, which is known as the action potential. Thus, if a nerve fiber measuring 12.8 µm in diameter is stimulated by a square stimulus pulse of 300 µs of duration and 2 V of amplitude, a

specific action potential is produced, as shown in Figure 2(b) (dark line). However, for a subthreshold stimulus (1.9V of amplitude), no action potential is produced (see Figure 2(b) (light line)), and the fiber is not activated.

Based on a previous study by Holsheimer (6), we considered two nerve fiber sizes. On the DC surface, 12.8-µm nerve fibers are the largest that can be activated. However, the DR nerve fibers can have a diameter of 15 µm. As the geometric parameters of 12.8- and 15-µm nerve fibers have been published (36), we used these fiber sizes in our simulations.

Histological data demonstrate that there are several nerve fiber sizes distributed in the DC (10,37). However, to simplify the simulation procedure, we only considered the 12.8-µm nerve fiber size. Therefore, in our model, the fiber distribution consisted of a set of 30 rows of 100 nerve fibers (a total of 3,000 fibers) spaced 50 µm apart and running from the DC surface to a depth of 2.25 mm (see blue zones in Figure 5 and Figure 6).

Simulation procedure

First, we determined electrode polarity by assigning contacts as cathodes or anodes. For this study, we considered common polarities used in single-lead stimulation: bipolar 1 (B1) (in which an anode is followed by a cathode), bipolar 2 (B2) (in which an anode and a cathode are separated by two inactive poles), guarded cathode (GC) (in which one cathode is programmed between anodes), and dual-guarded cathode (DGC) (in which two cathodes are programmed between anodes). In dual-lead stimulation, we used B1, GC, and DGC (see Figure 3).

Second, electric field distribution was simulated by solving the equations of the FEM model. We then exported a grid of points from COMSOL to MATLAB with the spatial position and the electric potential values of the nodes of Ranvier and solved the MRG model equations to obtain the first activated nerve fiber on the DC surface. If an action potential was obtained, the perception

threshold (PT) was achieved. If not, we increased the stimulation voltage by increments of 0.1 V, starting from zero, until the PT was achieved. The stimulation pulse applied consisted of a square-wave voltage pulse with a 300-μs duration. The stimulation threshold of the DR nerve fibers was also calculated.

The therapeutic range of stimulation between the PT and the level which causes the discomfort threshold (DT) is termed the usage range (UR) (22,38), which will generally not exceed 2PT (22). In clinical practice, a typical UR value ranges from 1.4 to 1.7 (7). Because the DC fibers in our simulations always had the lowest stimulation threshold, we used the PT from the DCs (PT_{DC}) to simulate neural activation at different DTs ($1.2PT_{DC}$, $1.4PT_{DC}$, and $1.8PT_{DC}$). We then used the MRG model to determine which nerve fibers in the DCs were activated.

Finally, the parameters listed below were calculated to compare the use of the different electrode polarities.

Evaluation parameters

To quantitatively compare the effect of different stimulation patterns on neural activation, we calculated several model output parameters defined as follows:

PT_{DC} (V): the lowest voltage needed to activate the first DC nerve fiber with a 12.8-μm diameter in our model. This value corresponds to the electrode potential that is expressed relative to a remote reference, that is, a stimulation threshold of 1 V in our model corresponds to a stimulation threshold of 2 V in our clinical practice.

PT_{DR} (V): the lowest voltage needed to activate the first DR nerve fiber with a 15-μm diameter in our model. This value corresponds to the electrode potential that is expressed relative to a remote reference, that is, a stimulation threshold of 1 V in our model corresponds to a stimulation threshold of 2 V in our clinical practice.

Activating area (mm^2): the maximum transversal area of the DCs within which DC nerve fibers are activated at $1.4PT_{DC}$.

Activating depth (μm): the maximum cross-sectional depth of the DCs within which DC nerve fibers are activated at $1.4PT_{DC}$. Depth is measured at the center of the recruitment contour.

Recruitment ratio ($R_{DC/DR}$): the ratio between PT_{DC} and PT_{DR}.

RESULTS

We analyzed and compared the effect of electrode polarity in single- and dual-lead stimulation. In Figure S1 of the Supporting Information section, the norm of the electric field at the surface of the white matter is represented for all previously described polarities. We also studied the effect of having different DTs in all polarities considered for both the activating area and depth in the spinal cord.

Model behavior

We reproduced two previous studies and compared our results with those from other research groups.

The first study consisted in analyzing the evolution of PT_{DC} versus dorsal CSF (dCSF) thickness. Holsheimer et al. (39) obtained PT_{DC} considering a nerve fiber measuring 12 μm in diameter. As displayed in Figure 4(a), our results showed that a higher dCSF thickness required a higher PT_{DC} (solid line), as also shown by Holsheimer et al. (dotted line). The absolute values of PT_{DC} were similar to Holsheimer's. The main difference was how fast PT_{DC} grew with dCSF thickness. Thus, for example, in our results, at maximum dCSF thickness (4.8 mm), PT_{DC} was 725% greater than at minimum dCSF thickness (0.8 mm) (5.8 V versus 0.8 V, respectively). However, Holsheimer et al. obtained an increase of 1,166% of PT_{DC} (7 V versus 0.6 V, respectively).

We also analyzed the effect of fiber diameter on PT_{DC}. The results are shown in Figure 4(b). Consistent with Holsheimer et al. (6) (dotted line), we found that the larger the nerve fiber diameter is, the lower the PT_{DC} required (solid line). Holsheimer et al. observed that their data points were best fitted by power function and showed the equation and the square correlation. We also verified that the best fit of our data points was by power function. We obtained the maximum difference of PT_{DC} (200% greater than the Holsheimer group results [9.8 V versus 4.88 V, respectively]) when a fiber measuring 5.7 μm in diameter is stimulated.

The differences observed in Figure 4(b) could arise from the differences between the models. On the one hand, Holsheimer's group used a T11 vertebral level, whereas we used a T10 vertebral level model. Each vertebral level has a different dCSF thickness, which is greater in the case of T10. On the other hand, we used an MRG nerve fiber model while Holsheimer's group used a Wesselink nerve fiber model in both studies. The main difference between the two models is that the myelin in the MRG model undergoes current losses because it is modeled as an imperfect insulator. Since these two differences could affect the excitability of the nerve fibers, they could explain the differences observed. Despite these distinctions, the behaviour of the model is very similar to that reported by Holsheimer's group, since both behave as a power function.

Single-lead stimulation

In this study, the electrode was positioned in the midline of the spinal cord at 0.1 mm from the dura mater. The dCSF was 4 mm thick, and four polarities were considered, namely, B1, B2, GC, and DGC (see Figure 3(a)).

First, we simulated the activating area and depth at three DT values ($1.2PT_{DC}$, $1.4\ PT_{DC}$, and $1.8\ PT_{DC}$) (see Figure 5). Figure 5 reveals that, regardless of the polarity considered, as DT increases,

both activating area and depth also increase. In addition, DGC and B2 are the polarities within which it is possible to obtain higher activating area and depth.

On the other hand, evaluation parameters were calculated at a DT of 1.4 PT_{DC} to quantitatively compare the effect of using different polarities. As we can see in Table 3, GC is the polarity with a better DC stimulation preference versus DR stimulation, with a $R_{DC/DR}$ of 0.38, although it produces the lowest activating area and depth values (1.5 mm^2 and 350 µm, respectively). Nevertheless, B1 and B2 present higher activating area and depth with the disadvantage that $R_{DC/DR}$ increases to 79% (0.68) and 110% (0.80), respectively, whereas the results show that DGC provides double the activating area and depth of GC with a reduction of 12.5% (1.4 V) in PT_{DC}. However, compared with GC, DGC polarity increases $R_{DC/DR}$ by 36% (0.52).

Dual-lead stimulation

Dual-lead stimulation is mainly used in complex pain patients, so we also modeled the use of different polarities (B1, GC, and DGC) (see Figure 3(b)) with dual leads positioned symmetrically 0.1 mm from the dura mater and with an axis-to-axis electrode separation of 2.5 mm, which is a commonly used distance between electrodes. The dCSF had a thickness of 4 mm.

The results show that dual-lead stimulation produces a higher lateral activation of the DC nerve fibers because neural activation is produced mainly under the cathode(s) (see Figure 6). However, this effect is reduced when DGC is used. As in a single-lead stimulation, it can be seen that, as DT increases (from 1.2PT_{DC} to 1.8PT_{DC}), the activating area and depth also increase in all polarities considered.

Next, we calculated the evaluation parameters at a DT of 1.4PT_{DC} (see Table 3). In terms of DR stimulation, GC is the polarity which most probably activates the DC nerve fibers, with a $R_{DC/DR}$ of 0.43. As a disadvantage, the activating area and depth are the lowest (1.24 mm^2 and 350 µm,

respectively). However, although B1 polarity increases the activating area by 21% (1.5 mm^2) and the activating depth by 14% (400 µm) as a result of increasing the PT_{DC} by 4% (2.4 V), the $R_{DC/DR}$ is 65% higher (0.71); therefore, the probability of activating DR nerve fibers is higher than it is for GC. Finally, compared to GC, the results show that DGC provides an increase of 113% for the activating area (2.64 mm^2) and of 57% for the activating depth (550 µm) with a reduction of 40% of PT_{DC} (1.4 V). The disadvantage is that the $R_{DC/DR}$ parameter is 42% higher (0.61).

Single vs. dual-lead stimulation

Figure 7 shows the evolution of the activating area and depth when the UR ratio increases for both single- and dual-lead stimulation. In general, single-lead stimulation produces a higher activating area in all polarities and in all usage range ratios than dual-lead stimulation. In addition, this difference is more evident as usage range ratio increase. For example, at a usage range of 1.2, the activating area of GC in dual-lead stimulation is 0.56 mm^2, while in single-lead stimulation it is 0.62 mm^2 (i.e. 10.7% higher). However, when usage range ratio increases to 1.8, the activating area in dual-lead stimulation is 3 mm^2 while in single-lead stimulation it is 4.65 mm^2 (i.e. 55% higher). The same effect has been observed with the activating depth when using single-lead stimulation, although this effect is not as evident for all polarities. For instance, GC presents the same activating area and depth in all usage range ratios, in both single- and dual-lead stimulation. Instead, DGC presents an activating depth of 250 µm in dual-lead stimulation at a usage range of 1.2, which increases to 300 µm (50 µm deeper) in single-lead stimulation. Furthermore, in this case it is also seen that when usage range ratio increases, this effect is more evident. Therefore, at a usage range of 1.8, the activating depth in dual-lead stimulation is 1000 µm, which increases to 1100 µm (100 µm deeper) in single-lead stimulation.

The effect of using asymmetrical polarities produces a lateral activation on DC, as seen in Figure 6. Consequently, as the neural activation is produced under the active electrode, the activating area is reduced compared with single-lead stimulation, due to the lateral position of the electrodes. The activation depth, however, is also lower, but the decrease is not as evident as the decrease in the activating area.

Despite the differences observed between single- and dual-lead stimulation, in both cases, it is shown that DGC maximizes the activating area and depth in comparison with the other polarities. Moreover, the difference is higher as the usage range ratio increases. Nevertheless, the effect of stimulation using two leads instead of one appears not to produce, theoretically, higher activating area or depth.

DISCUSSION

The modeling study we present quantitatively compares the effect of electrode polarity (in single- and dual-lead stimulation) on neural activation in SCS therapy and determines which one maximizes the activation area and depth in DC. To the best of our knowledge, there are some works that also studied the effect of polarity in SCS (11,13,22,30) and even the effect of using a multiple current versus single current source stimulation (40,41). However, this is the first study that considers and compares the effect of the most known and used electrode polarities in single- and dual-lead stimulation (B1, B2 and GC) including, in addition, DGC polarity, which has never been compared to the previous polarities in SCS therapy.

We developed a new 3D spinal cord model that includes the following novel aspects. First, the geometry of the model is based on measurements of all spinal cord levels from high-resolution *in vivo* T2*-weighted magnetic resonance images acquired at 3T (24). Therefore, as in a real spinal

cord, the white matter is not centered within the spinal canal in our spinal cord model. This is an important contribution, since it enables us to see that, owing to the midline offset of the white matter modeled, even in single-lead stimulation, the activating area is not central, but lateral. However, previous models, besides not including the midline offset of the white matter, used anatomical data taken from the rat spinal cord atlas (42), postmortem measurements of human spinal cord (26), or *in vivo* human measurements at some vertebral levels (C4-C6, T5-T6 and T11-T12) from low-resolution *in vivo* T2*-weighted magnetic resonance images acquired at 1.5T (11,13,23). The second novel aspect is that our model is the first to include the electrode-tissue interface around the active contacts of the electrode in a spinal cord model. It is important to consider this element, because it affects the stimulation threshold values of the nerve fibers and, therefore, the remaining evaluating parameters.

In this computer modelling study, we compared four polarities (B1, B2, GC, and DGC) in single-lead stimulation and three polarities in dual-lead stimulation (B1, GC and DGC). To date, the most commonly analyzed polarities have been B1, B2, and GC (43,44). Thus, several studies from Holsheimer's group proved that GC produced the greatest recruitment of DC fibers and the widest paresthesia coverage (13,22,43,44). However, the effect of DGC polarity has never been compared with that of the other polarities in SCS. This effect has only been evaluated in a peripheral nerve field stimulation study from Frahm et al. (45), where DGC presented a larger activating area than GC, and in a cathodal field steering study from Manola et al. (11), where DGC showed extended recruitment of DC fibers as compared with dual cathode (two consecutive cathodes without anodes). Therefore, given the lack of studies on the effect of electrode polarity in SCS and the wider paresthesia coverage obtained empirically using DGC in our clinical practice, we included DGC polarity in this study. In addition, in the case of dual-lead stimulation, we considered asymmetrical polarities, since, based on our clinical experience, it is difficult to produce the same

intensity of tingling sensation on both sides of the patient's body when symmetrical polarities are used. This is because perception thresholds are usually different on both sides of the body, since they depend on the position of the electrodes and the geometry of the spinal cord, i.e., the midline offset of the white matter. However, asymmetrical polarities enable us to adapt the stimulation parameters for each side of the body and produce better paresthesia coverage. Thus, in this study we were interested in comparing the effect of using the most used and known polarities in single-lead stimulation versus the most used asymmetrical polarities in our clinical practice in dual-lead stimulation.

Therefore, we compared four polarities (B1, B2, GC, and DGC) in single-lead stimulation. In terms of activating area and depth, the results showed that DGC performed the best. B1 and B2 polarities also achieved high activating area and depth, but DR stimulation was more easily produced. This effect was previously found by Barolat et al. (45), who observed that narrower spacing between bipolar contacts increased DC fiber selectivity. In dual-lead stimulation, we compared three polarities (B1, GC, and DGC) and observed the same effect: DGC produced the highest activating area and depth.

However, in terms of $R_{DC/DR}$ in single and dual-lead stimulation, the best performing polarity was GC, since it presented the lowest value, meaning that it is less likely to activate DR nerve fibers, as predicted in previous studies (7,13,22,46). In addition, B2 (in single-lead stimulation) and B1 (in dual-lead stimulation) presented the highest $R_{DC/DR}$ value; therefore, these polarities were likely to stimulate DR nerve fibers, reducing paresthesia coverage to only two dermatomes and producing a stimulation which would not be sufficient to cover all pain dermatomes.

We also compared the use of single- and dual-lead stimulation. The results show that dual-lead stimulation produces higher lateral activation with less depth than that of a single-lead, as

Holsheimer suggested (47). Furthermore, PT_{DR} is reduced because electrodes are more laterally placed and the distance between DR and the electrodes is shorter. Thus, the recruitment ratio is higher than that obtained in single-lead stimulation, which is in agreement with Struijk et al. (17) and Holsheimer et al. (39). However, according to a clinical study by Aló et al. (48), the advantage of dual-lead stimulation is that it could optimize long-term SCS paresthesia overlap.

Therefore, the comparison of the effect of the electrode polarity used in this study is the first to prove that, compared to B1, B2 and GC, DGC could achieve the maximum activating area and depth in both single- and dual-lead stimulation, and thus, the widest paresthesia coverage in SCS therapy.

In our clinical practice, polarity is established by trial and error and asking the patient about the location of the tingling sensation. In addition, polarity is the first parameter to be programmed, because it determines the electric field, and therefore, the location of the nerve fibers that will be activated. By selecting this location, we select the dermatomes we wish to activate. Then, according to our results, a new strategy is proposed to establish polarity. The strategy consists first in using DGC, in single- and dual-lead stimulation, with the aim of maximizing the activating area and depth. However, in cases where DR activation is produced first, the results point to GC. This strategy would enable more effective stimulation, since paresthesia coverage would also be maximized.

Model limitations

One of the main limitations of SCS research is the lack of available clinical data. Clinical studies are complicated to perform owing to the highly subjective and sensitive nature of the data obtained from the patient's sensations. Thus, to date, it has been not possible to clinically validate the model presented in this article. Further research would require clinical data from a specific group

of patients (with a specific age, sex, disease, electrode geometry, and position in the vertebral level) to clinically validate the computational model. This would provide more accurate and realistic SCS models because computer modeling helps us to understand SCS effects, improve stimulating parameters, and know how to design better electrodes and devices (49).

Second, lead position in the computational model is unrealistic, in the sense that it is perfectly situated in the midline of the spinal cord (in single-lead stimulation) or symmetric (in dual-lead stimulation). These positions are complicated to reproduce in a real patient, because it is not possible to know the exact location of the physiologic midline of the spinal cord in each patient.

Moreover, nerve fiber distribution within the DC is a complex feature, which requires further research. In current mathematical models, some studies use several nerve fiber sizes (13,50), whereas others maintain a fixed nerve fiber size distribution (11,26). This uncertainty of how fiber size changes with depth affects both activating area and depth.

Finally, the nerve fiber model used does not consider any connectivity between nerve fibers. It is possible that the activation of one nerve fiber contributes to the activation of other nerve fibers positioned around it. If this assumption is proven to be true, the results reported may be affected, because the stimulation threshold values (PT_{DC} and PT_{DR}) would probably be reduced, and the remaining parameters ($R_{DC/DR}$, activating area and depth) that depend on these values would be different. Therefore, in order to have a more realistic model of the spinal cord, nerve fiber connectivity would have to be considered in further studies. However, the inclusion of this new feature in the model would not affect the main conclusions of the present study.

CONCLUSIONS

Broad knowledge of the effect of electrode polarity on neural activation in SCS could help clinicians to perform more efficient stimulations in chronic pain treatment. This study is the first to quantitatively compare the effect of the most known and used electrode polarities (B1, B2 and GC) on neural activation in single- and dual-lead stimulation in SCS, including DGC polarity, which has never been compared to the previous polarities.

The results obtained from our 3D spinal cord model suggest that DGC polarity could maximize neural activation, both in single- and dual-lead stimulation. Therefore, based on the results obtained, we propose a new strategy to maximize the activating area and, thus, paresthesia coverage in clinical practice. This strategy would consist of initially using DGC polarity in single- and dual-lead stimulation to obtain the maximum activating area in the DC. However, if the DR was activated, then paresthesia coverage would be reduced to only one or two dermatomes. This could result in inefficient stimulation for the patient in terms of paresthesia coverage. Therefore, in these cases, the appropriate following step would be to use GC polarity to ensure DC nerve fiber activation, owing to its low recruitment ratio.

ACKNOWLEDGEMENTS

The authors thank Virginie Callot for providing us with all the spinal cord measurements from her research group's study. The authors would like also to thank Surgicen S.L. for providing financial assistance.

REFERENCES

1. Shealy CN, Mortimer JT, Reswick JB. Electrical inhibition of pain by stimulation of the dorsal columns. Anesth Analg. 1967;46(4):489–91.

2. Simpson BA. Spinal cord stimulation. Br J Neurosurg. 1997;11(1):5–11.

3. North RB, Kidd DH, James C, Long D. Spinal cord stimulation for chronic, intractable pain: experience over two decades. Neurosurgery. 1993;32(3):384–95.

4. Epstein LJ, Palmieri M. Managing chronic pain with spinal cord stimulation. Mt Sinai J Med A J Transl Pers Med. 2012;76(1):123–32.

5. Kumar K, Taylor RS, Jacques L, Eldabe S, Meglio M, Molet J, et al. The effects of spinal cord stimulation in neuropathic pain are sustained: a 24-month follow-up of the prospective randomized controlled multicenter trial of the effectiveness of spinal cord stimulation. Neurosurgery. 2008;63(4):762–70.

6. Holsheimer J. Which neuronal elements are activated directly by spinal cord stimulation. Neuromodulation. 2002;5(1):25–31.

7. Molnar G, Barolat G. Principles of cord activation during spinal cord stimulation. Neuromodulation Technol Neural Interface. 2014;17:12–21.

8. Melzack R, Wall P. Pain mechanisms: a new theory. Science (80-). 1965;150(3699):971–9.

9. Oakley J, Prager JP. Spinal cord stimulation: Mechanisms of action. Spine (Phila Pa 1976). 2002;27(22):2574–83.

10. Feirabend HKP, Choufoer H, Ploeger S, Holsheimer J, van Gool JD. Morphometry of human superficial dorsal and dorsolateral column fibres: significance to spinal cord stimulation. Brain. 2002;125:1137–49.

11. Manola L, Holsheimer J, Veltink PH, Bradley K, Peterson D. Theoretical investigation into longitudinal cathodal field steering in spinal cord stimulation. Neuromodulation Technol Neural Interface. 2007;10(2):120–32.

12. Linderoth B, Foreman RD. Conventional and novel spinal stimulation algorithms: hypothetical mechanisms of action and comments on outcomes. Neuromodulation Technol

Neural Interface. 2017;20(6):525–33.

13. Manola L, Holsheimer J, Veltink P. Technical performance of percutaneous leads for spinal cord stimulation: A modeling study. Neuromodulation Technol Neural Interface. 2005;8(2):88–99.

14. Vallejo R, Bradley K, Kapural L. Spinal cord stimulation in chronic pain. Spine (Phila Pa 1976). 2017;42(14):S53–60.

15. Rao SS. Overview of finite element method. In: The Finite Element Method in Engineering. Fourth. Elsevier Science & Technology Books; 2004. p. 3–53.

16. Holsheimer J. Computer modelling of spinal cord stimulation and its contribution to therapeutic efficacy. Spinal Cord. 1998;36:531–40.

17. Struijk JJ, Holsheimer J, Boom HBK. Excitation of dorsal root fibers in spinal cord stimulation : a theoretical study. IEEE Trans Biomed Eng. 1993;40(7):632–9.

18. Struijk JJ, Holsheimer J, van der Heide GG, Boom HB. Recruitment of dorsal column fibers in spinal cord stimulation: influence of collateral branching. IEEE Trans Biomed Eng. 1992;39(9):903–12.

19. Holsheimer J, Raza SS. Effects of electrode positioning on perception threshold and paresthesia coverage in spinal cord stimulation. Neuromodulation Technol Neural Interface. 2007;10(1):34–41.

20. He J, Barolat G, Holsheimer J. Perception threshold and electrode position for spinal cord stimulation. Pain. 1994;59:55–63.

21. Gordon AT, Zou SP, Kim Y, Gharibo C. Challenges to setting spinal cord stimulator parameters during intraoperative testing: factors affecting coverage of low back and leg pain. Neuromodulation Technol Neural Interface. 2007;10(2):133–41.

22. Holsheimer J, Wesselink WA. Effect of anode-cathode configuration on paresthesia

coverage in spinal cord stimulation. Neurosurgery. 1997;41(3):654–60.

23. Fradet L, Arnoux P, Ranjeva J, Petit Y, Callot V. Morphometrics of the entire human spinal cord and spinal canal measured from in vivo high resolution anatomical magnetic resonance imaging. Spine (Phila Pa 1976). 2014;39(4):E262–9.

24. Reina MA, López-García A, Dittman M, de Andrés JA. Análisis estructural del espesor de la duramadre humana mediante microscopía electrónica de barrido. Rev Esp Anestesiol Reanim. 1996;43:135–7.

25. Westbrook JL, Renowden S a., Carrie LES. Study of the Anatomy of the Extradural Region Using Magnetic Resonance Imaging. BJA Br J Anaesth. 1993;71(4):495–8.

26. Arle JE, Carlson KW, Mei L, Shils JL. Modeling effects of scar on patterns of dorsal column stimulation. Neuromodulation Technol Neural Interface. 2014;17:320–33.

27. Ladenbauer J, Minassian K, Hofstoetter US, Dimitrijevic MR, Rattay F. Stimulation of the human lumbar spinal cord with implanted and surface electrodes: A computer simulation study. IEEE Trans Neural Syst Rehabil Eng. 2010;18(6):637–45.

28. Collaboration for NDT Education. Conductivity and Resistivity Values for Nickel & Alloys [Internet]. Technology. 2002. Available from: https://www.nde-ed.org/GeneralResources/MaterialProperties/ET/Conductivity_Misc.pdf

29. Mcintyre CC, Mori S, Sherman DL, Thakor N V, Vitek JL. Electric field and stimulating influence generated by deep brain stimulation of the subthalamic nucleus. Clin Neurophysiol. 2004;115:589–95.

30. Sankarasubramanian V. Model-based stimulation optimization for chronic pain supression using percutaneous and surgical leads in spinal cord stimulation (SCS). [Enschede, The Netherlands]: University of Twente; 2013.

31. Huang Q, Oya H, Flouty OE, Reddy CG, Howard MA, Gillies GT, et al. Comparison of spinal

cord stimulation profiles from intra- and extradural electrode arrangements by finite element modelling. Med Biol Eng Comput. 2014;52(6):531–8.

32. Medtronic. Vectris SureScan MRI 1x8 Compact. Implant manual [Internet]. Minneapolis, MN 55432-5604, USA; 2013. p. 10–1. Available from: http://manuals.medtronic.com/content/dam/emanuals/neuro/CONTRIB_220954.pdf

33. Butson CR, Mcintyre CC. Current steering to control the volume of tissue activated during deep brain stimulation. Brain Stimul. 2008;1:7–15.

34. Butson CR, Maks CB, Mcintyre CC. Sources and effects of electrode impedance during deep brain stimulation. Clin Neurophysiol. 2006;117:447–54.

35. Richardson AG, Mclntyre CC, Grill WM. Modelling the effects of electric fields on nerve fibres: influence of the myelin sheath. Med Biol Eng Comput. 2000;38:438–46.

36. Mcintyre CC, Richardson AG, Grill WM. Modeling the excitability of mammalian nerve fibers: influence of afterpotentials on the recovery cycle. J Neurophysiol. 2002;87:995–1006.

37. Wesselink WA, Holsheimer J, Nuttin B, Boom HBK, King GW, Gybels JM, et al. Estimation of fiber diameters in the spinal dorsal columns from clinical data. IEEE Trans Biomed Eng. 1998;45(11):1355–62.

38. Barolat HJ, Ketcik B G. Stimulation usage range for chronic pain management. Analgesia. 1995;1:75–80.

39. Holsheimer J, Buitenweg JR. Review: bioelectrical mechanisms in spinal cord stimulation. Neuromodulation Technol Neural Interface. 2014;18:161–70.

40. Lee D, Gillespie E, Bradley K. Dorsal column steerability with dual parallel leads using dedicated power sources: a computational model. J Vis Exp. 2011;(48):2–5.

41. Xiaoyi Min X, Kent AR, Rosenberg SP, Fayram TA. Modeling dermatome selectivity of single-

and multiple-current source spinal cord stimulation systems. In: 2014 36th Annual International Conference of the IEEE Engineering in Medicine and Biology Society [Internet]. IEEE; 2014 [cited 2018 Oct 24]. p. 6246–9. Available from: http://www.ncbi.nlm.nih.gov/pubmed/25571424

42. Capogrosso M, Wenger N, Raspopovic S, Musienko P, Beauparlant J, Luciani LB, et al. A Computational Model for Epidural Electrical Stimulation of Spinal Sensorimotor Circuits. 2013;33(49):19326–40.

43. Holsheimer J, Struijk JJ, Tas NR. Effects of electrode geometry and combination on nerve fibre selectivity in spinal cord stimulation. Med Biol Eng Comput. 1995 Sep;33(5):676–82.

44. Holsheimer J, Struijk JJ, Wesselink WA. Effects of electrode configuration and geometry on fiber preference in spinal cord stimulation. In: 18th Annual International Conference of the IEEE Engineering in Medicine and Biology Society. Amsterdam; 1996. p. 343–4.

45. Barolat G, Zeme S, Ketcik B. Multifactorial analysis of epidural spinal cord stimulation. Stereotact Funct Neurosurg. 1991;56(2):77–103.

46. North RB, Ewend MG, Lawton MT, Piantadosi S. Spinal cord stimulation for chronic, intractable pain: superiority of “multi-channel” devices. Pain. 1991;44(2):119–30.

47. Holsheimer J. Does dual lead stimulation favor stimulation of the axial lower back? Neuromodulation. 2000;3(2):55–7.

48. Aló KM, Redko V, Charnov J. Four year follow-up of dual electrode spinal cord stimulation for chronic pain. Neuromodulation. 2002;5(2):79–88.

49. Grill WM, Howell B. Systems and methods for model-based optimization of spinal cord stimulation electrodes and devices. U.S. Patent Application No. 15/321, 801, 2017.

50. Lee D, Hershey B, Bradley K, Yearwood T. Predicted effects of pulse width programming in spinal cord stimulation: a mathematical modeling study. Med Biol Eng Comput.

2011;49:765–74.

SUPPORTING INFORMATION

Table S1 shows the geometric parameters used in the MRG model of the nerve fibers considered in DC and DR structures.

Table S2 presents the electrical parameters of the ion channels, the myelin and the node of Ranvier used in the MRG model.

In Table S3, the equations of the membrane currents and the electric potential of the MRG model are given.

Table S4 shows the equations of the gate probabilities and coefficients. The dynamics of the MRG model are defined at 20°C. The adequate Q_{10} scaling factors are also indicated for each of the activation and inactivation parameters.

Figure S1 shows the norm of the electric field in the surface of the white mater for B1, B2, GC and DGC polarities in single-lead stimulation; and for B1, GC and DGC polarities in dual-lead stimulation. It demonstrates that asymmetric polarities in dual-lead stimulation can move the electric field to the lateral of the spinal cord. Moreover, this effect is more evident when an anode is programmed in front of a cathode, as it can be seen in the DGC polarity.

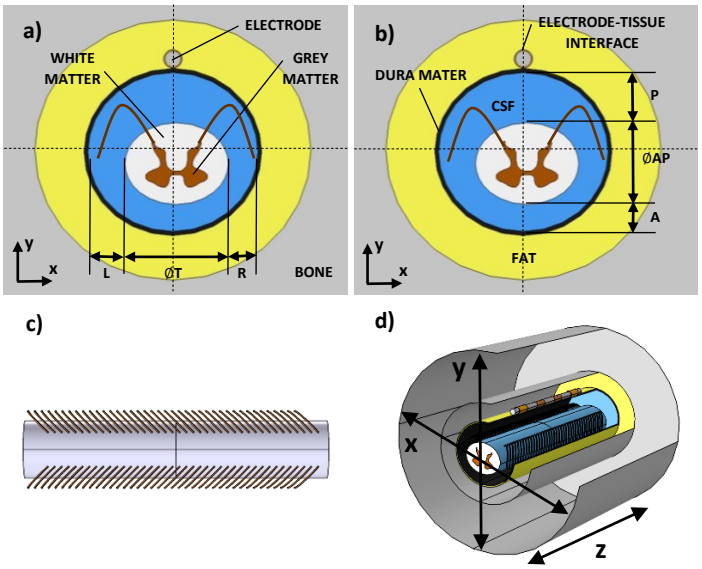

Figure 1. a) Geometric parameters of the T10 vertebral level of the spinal cord model (R: 2.4 mm, L: 3 mm, ØT: 8.4 mm) obtained from (23) and spinal cord tissues considered in the FEM model (grey matter, white matter, bone and electrode). b) Geometric parameters of the T10 vertebral level of the spinal cord (P: 4 mm, A: 1.8 mm, ØAP: 6.6 mm) obtained from (23) and spinal cord tissues considered in FEM model (dura mater, CSF, fat and electrode-tissue interface). c) DR modeling. d) Model dimensions: *x*: 45mm, *y*: 42 mm and *z*: 44 mm. ØAP indicates anteroposterior diameter; ØT, transverse diameter; A, anterior; P, posterior; R, right; L, left; CSF, cerebrospinal fluid.

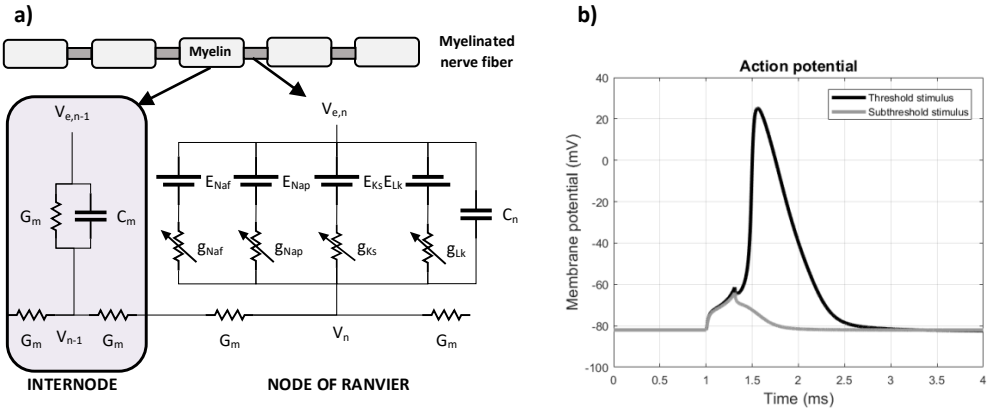

Figure 2. a) Schematic diagram of myelinated nerve fiber and equivalent electric circuit. b) Action potential when the nerve fiber is stimulated at threshold stimulus (dark line) and at subthreshold stimulus (light line).

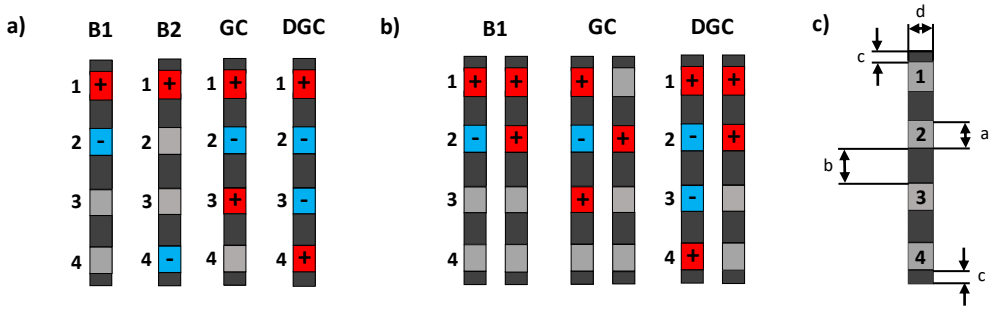

Figure 3. Leads polarity considered for: a) single-lead stimulation and b) dual-lead stimulation. Positive symbols represent the anodes (positive voltage) and negative symbols represent the cathodes (negative voltage). B1: bipolar 1, B2: bipolar 2, GC: guarded cathode and DGC: dual-guarded cathode. c) Geometric parameters of the lead size: contact length (a) is 3 mm; insulator length (b) is 4 mm; insulator length in the extremes (c) is 1.5 mm and lead diameter (d) is 1.3 mm.

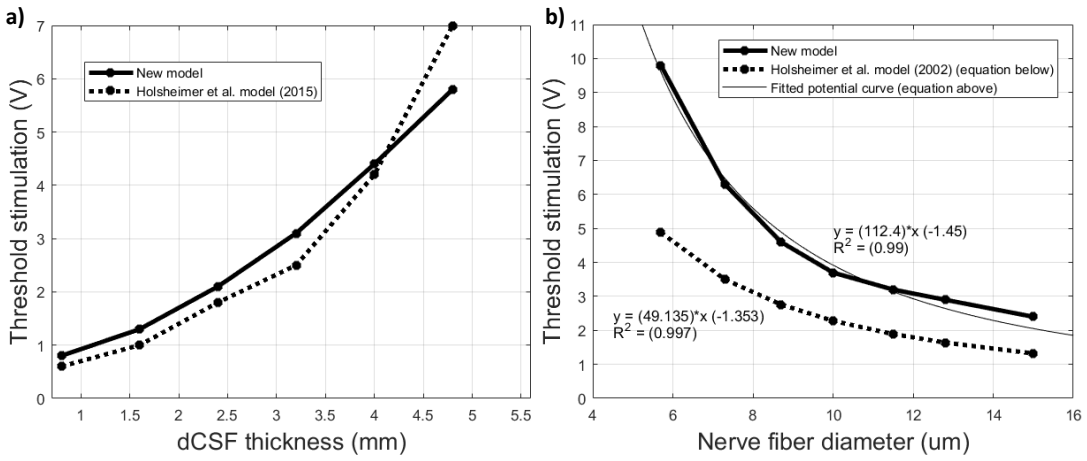

Figure 4. a) Threshold stimulation as a function of dCSF thickness. Solid line: results obtained using our model. Dotted line: results from Holsheimer's group (39). b) Threshold stimulation as a function of nerve fiber diameter. Solid line: results obtained using our model. Dotted line: results from Holsheimer's group (6).

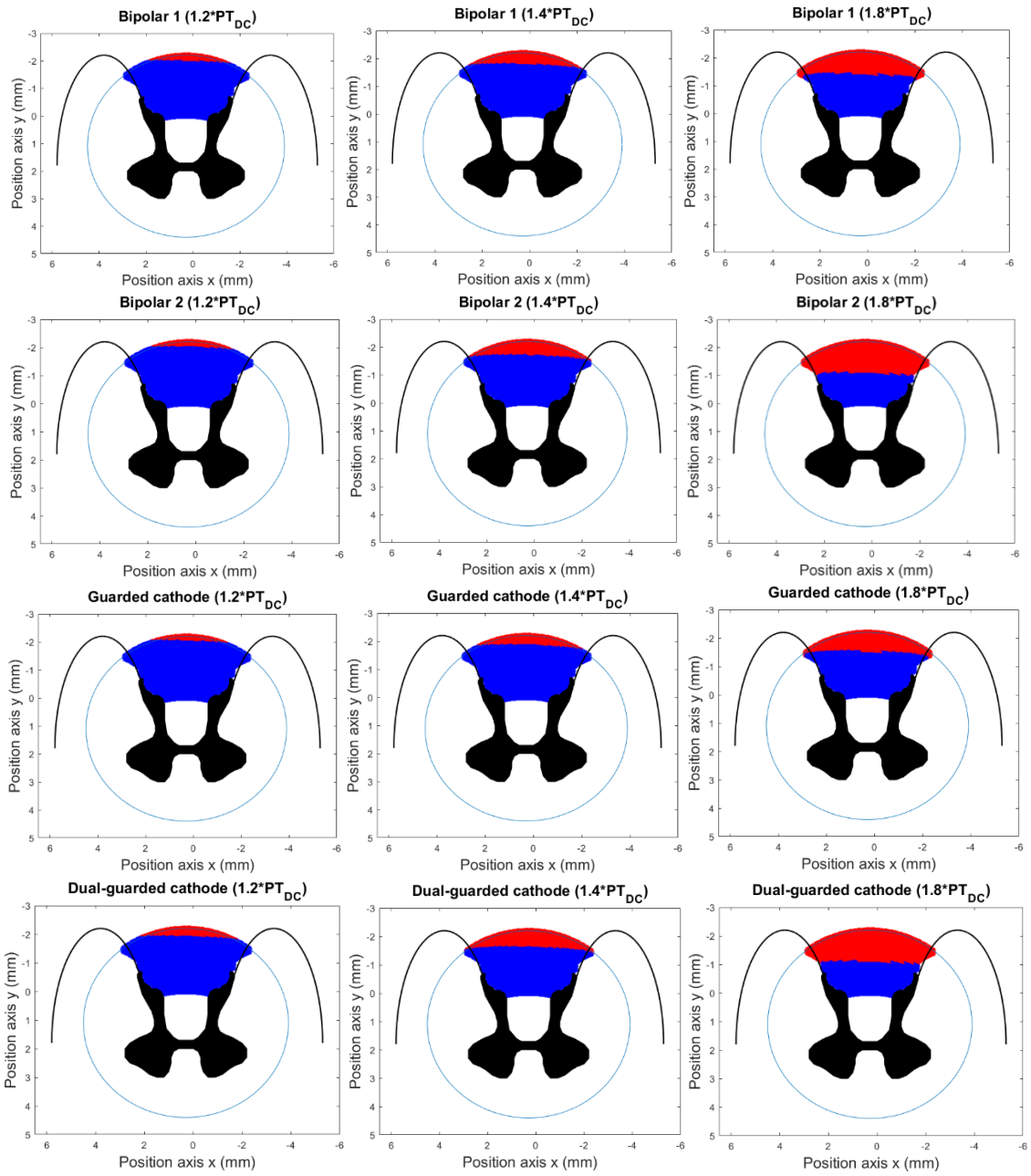

Figure 5. Activation area and depth obtained in different single lead polarities in the DC at different DTs (1.2PT$_{DC}$, 1.4PT$_{DC}$, and 1.8PT$_{DC}$). Blue zones (■) represent the nerve fibers that are not activated and red zones (■) represent the activated nerve fibers.

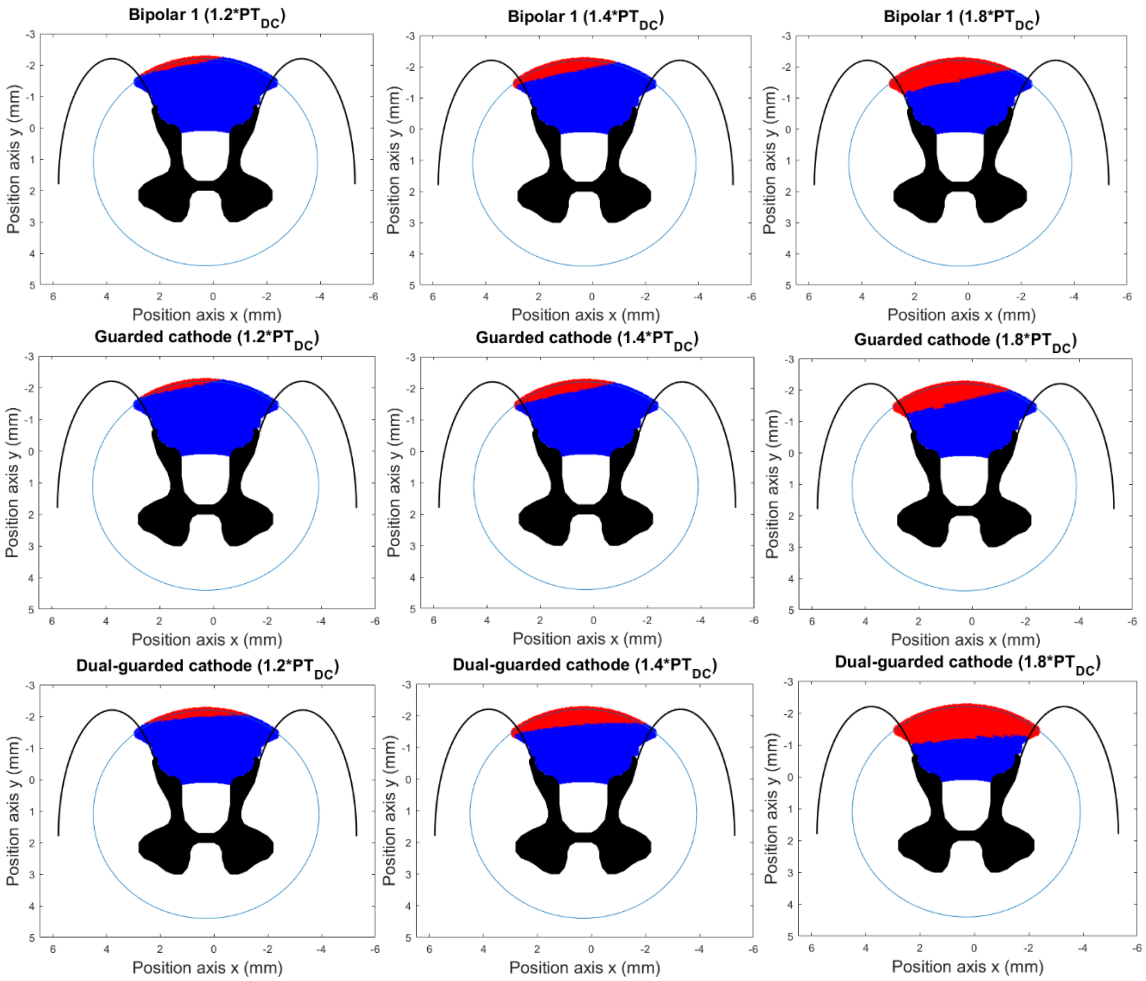

Figure 6. Activation area and depth obtained in some dual lead polarities in the DC at different DTs (1.2PT$_{DC}$, 1.4PT$_{DC}$, and 1.8PT$_{DC}$). Blue zones (■) represent the nerve fibers that are not activated and red zones (■) represent the activated nerve fibers.

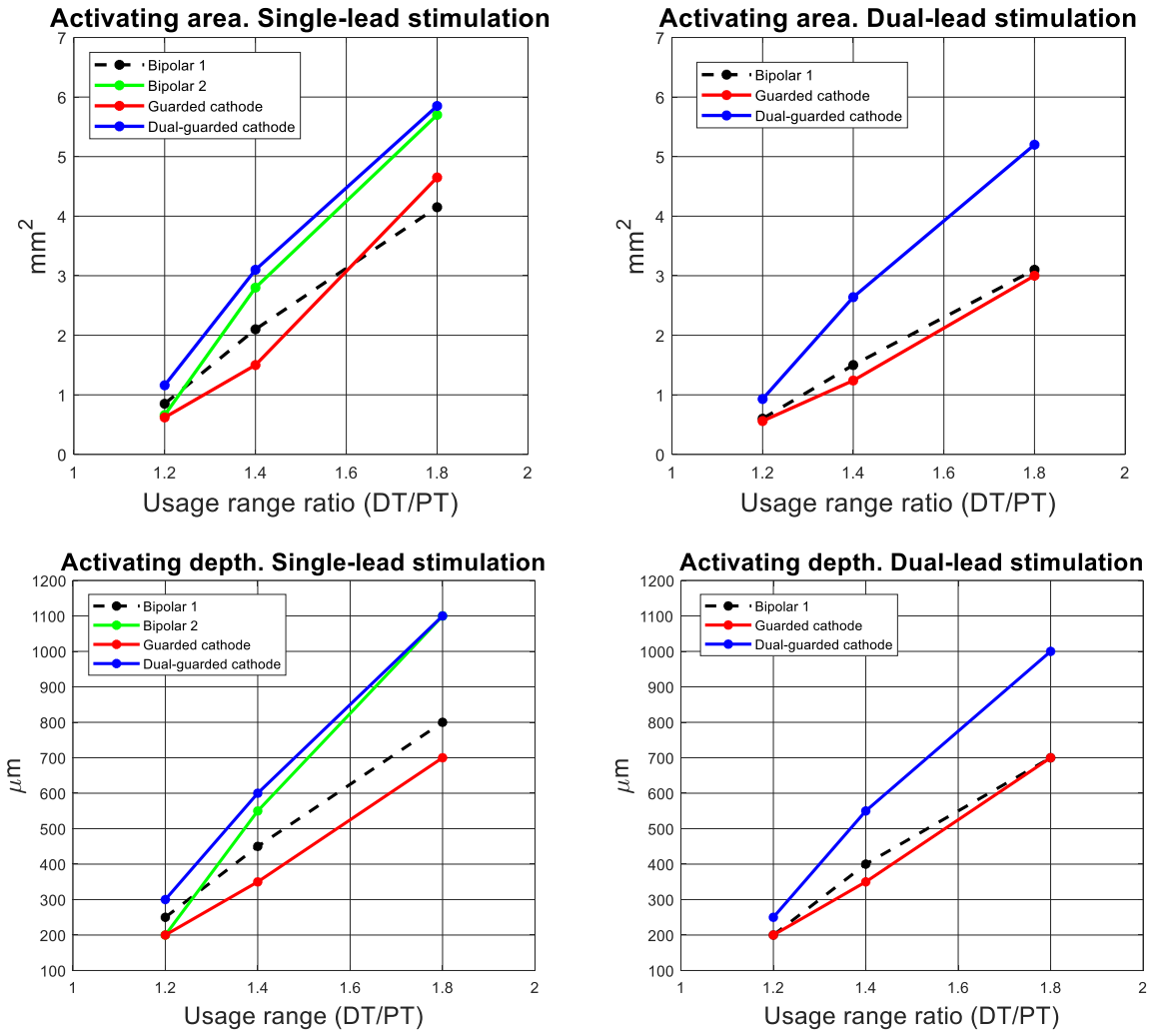

Figure 7. Activating area (up) and activating depth (down) in a single-lead (left) and dual-lead stimulation (right) as a function of the usage range ratio.

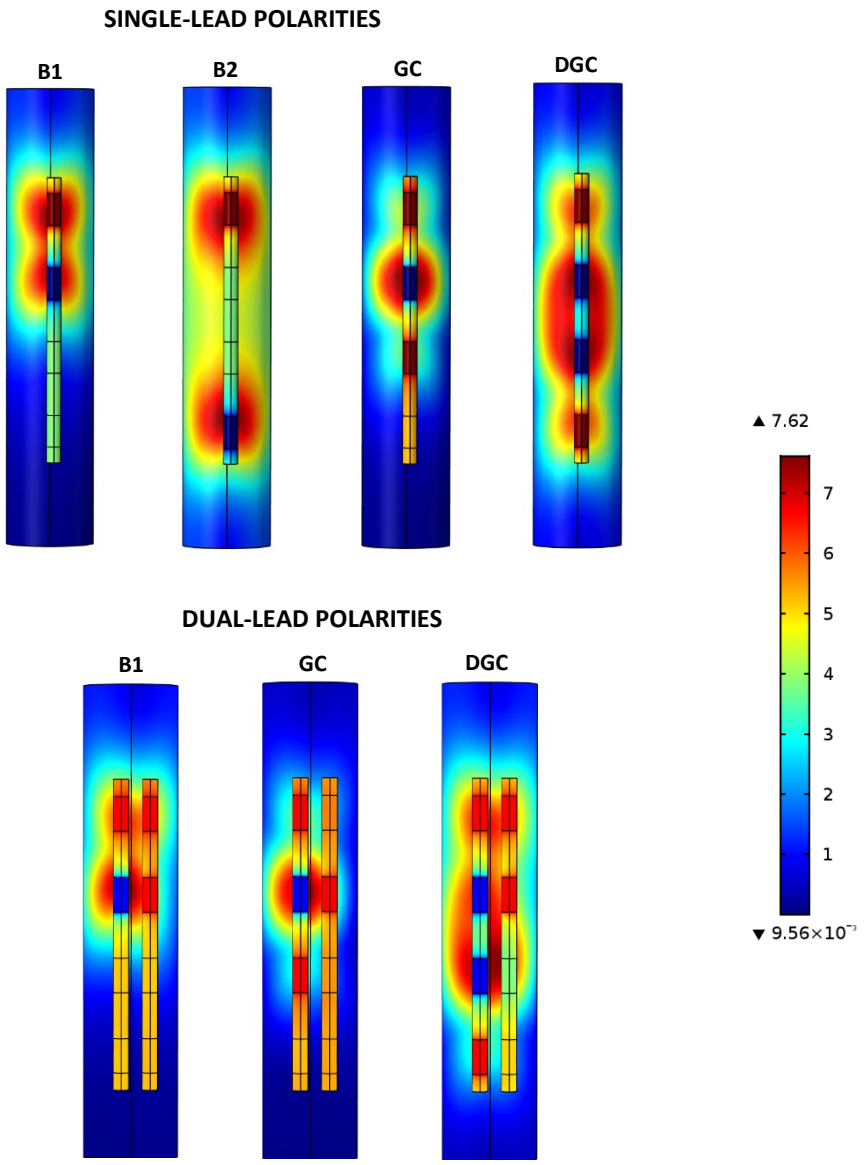

Figure S1. Electric field norm (V/m) produced on the surface of the white mater in different single- and dual-lead polarities. In the electrodes, anodes are represented in red color and cathodes are represented in blue color. The electric field norm is obtained at 1 V (1 V in the anodes and -1 V in the cathodes).